

1 Can irregularities of solar proxies help understand 2 quasi-biennial solar variations?

3
4 **A. Shapoval^{1,3,4}, J.L. Le Mouél², M. Shnirman^{1,2}, V. Courtillot²**

5 [1] {IEPT RAS, Profsoyuznaya str. 84/32, 117997, Moscow, Russia}

6 [2] {IPGP, 1 rue Jussieu, 75005, Paris, France}

7 [3] {Financial University, Leningradsky pr. 49, 125167, Moscow, Russia}

8 [4] {National Research University Higher School of Economics, 20 Myasnitskaya Ulitsa,
9 Moscow 101000, Russia}

10 Correspondence to: V. Courtillot (courtil@ipgp.fr), (tel. +(33)183957491)

11

12 **Abstract**

13 We define, calculate and analyze irregularity indices λ_{ISSN} ~~and λ_{aa}~~ of daily series of the
14 International Sunspot Number *ISSN* ~~and geomagnetic index *aa*~~ as a function of increasing
15 smoothing from $N = 162$ to 648 days. The irregularity indices λ are computed within 4-year
16 sliding windows, with embedding dimensions $m = 1$ and 2. λ_{ISSN} ~~and λ_{aa}~~ -displays Schwabe
17 cycles with sharp peaks not only at cycle maxima but also at minima: we call the resulting
18 ~ 5.5 -year variations "*half Schwabe variations*" (HSV). The mean of λ_{ISSN} undergoes a
19 downward step and the amplitude of its variations strongly decreases around 1930. We
20 observe changes in the ratio R of the mean amplitude of λ peaks at solar cycle minima with
21 respect to peaks at solar maxima as a function of date, embedding dimension and importantly
22 smoothing parameter N . We identify two distinct regimes, called Q1 and Q2, defined mainly
23 by the evolution of R as a function of N : Q1, with increasing HSV behavior and R value as N
24 is increased, occurs before 1915-1930 and Q2, with decreasing HSV behavior and R value as
25 N is increased, occurs after ~ 1975 . We attempt to account for these observations with an
26 autoregressive (order 1) model with Poissonian noise and a mean modulated by two sine
27 waves of periods T_1 and T_2 ($T_1 = 11$ years, and intermediate T_2 is tuned to mimic quasi-
28 biennial oscillations QBO). The model can generate both Q1 and Q2 regimes. When $m = 1$,

1 HSV appears in the absence of T_2 variations. When $m = 2$, Q1 occurs when T_2 variations are
2 present, whereas Q2 occurs when T_2 variations are suppressed. We propose that the HSV
3 behavior of the irregularity index of *ISSN* may be linked to the presence of strong QBO before
4 1915-1930, a transition and their disappearance around 1975, corresponding to a change in
5 regime of solar activity.

6

7 **1 Introduction**

8 Regular and irregular features of solar activity reflect the behavior of the solar dynamo. Their
9 spectrum contains low-frequency “cycles”, from decadal to centennial scales, whose durations
10 and amplitudes vary with time, and a higher frequency spectrum with much stronger
11 irregularities, notably in the 1 to 3 year pseudo-period range. The case of quasi-biennial
12 oscillations (QBO) have been widely discussed in the recent literature (e.g. McIntosh, et al.,
13 1992; Lawrence, et al., 2008; Mursula et al., 2003; Rouillard and Lockwood, 2004). The
14 range of 1 to 3 year quasi-periodicities has been studied in a number of time series, using
15 different techniques such as power spectral analysis (Rouillard and Lockwood, 2004; Valdes-
16 Galicia et al., 1996), wavelet analysis (Kudela et al., 2002; Mursula et al. , 2003), empirical
17 mode decomposition (Vecchio et al., 2010), or the successive approximation technique
18 (Mavromichalaki et al., 2003). All techniques confirm the reality of these quasi-periodicities,
19 with time-varying amplitude and “frequency”.

20 Several papers discuss variations with periods close to 27 days (related to the Sun’s rotation
21 as seen from Earth). For instance, in an earlier paper (Le Mouél et al., 2007), we considered
22 the series of the International Sunspot Number (*ISSN*) and magnetic *aa* index: we computed
23 their energy for periods around 27 days and found that this energy roughly followed the initial
24 time series it was computed from. More detailed analysis revealed a significant increase of
25 energy approximately two decades prior to the increase in solar activity that occurred in the
26 1930s. Other papers deal with the long-term evolution of short-term variations of different
27 time series by standard wavelet analysis (Lawrence et al., 2008) or using some modification
28 of Kolmogorov entropy (Blanter et al., 2005; Blanter et al., 2006). These papers reveal the
29 existence of different regimes in the long-term evolution of the high-frequency part of the
30 spectrum (estimated locally in time).

1 In a previous paper (Shapoval et al, 2013), we introduced the irregularity index of a given
2 time series as the convergence (or divergence) rate of nearby points in a certain phase space,
3 under a “one-step” translation. In the case of low-dimensional dynamical systems, the
4 irregularity index corresponds to the maximal Lyapunov exponent (e.g. Bergé et al., 1984).
5 Lyapunov exponents characterize the convergence (resp. divergence) rate of infinitesimally
6 close trajectories of a dynamical system to (resp. from) its attractor in phase space. There is a
7 link between the magnitude of the Lyapunov exponent and the regularity of the process: the
8 larger the exponent, the stronger the irregularities. In contrast to the maximal Lyapunov
9 exponent, the irregularity index can be computed for shorter time series with a significant
10 random component.

11 In Shapoval et al (2013), we explored variations of the irregularity index $\lambda_m(t)$ of the daily
12 *ISSN* series as a function of time for intermediate values (4 to 6) of the embedding dimension
13 m : $\lambda_m(t)$ generally attains strong main maxima at *ISSN* minima, has secondary maxima at
14 *ISSN* maxima and minima at the time of the descending and ascending phases of the Schwabe
15 cycles. Such a pattern of “half-Schwabe cycles”, with a large amplitude of λ main maxima,
16 remained stable between 1850 and 1915, then changed to a new pattern (with significantly
17 smaller maxima) that remained stable from 1935 to 2005. We interpreted this pattern change
18 as an indication of a “hidden” change in the regime of solar activity, the years 1915 to 1935
19 being a transitional interval. We could reproduce the observed behavior of λ with a synthetic
20 signal, consisting of an autoregressive process of order 1 with Poisson noise, modulated by an
21 11-year sine. The switch between the two regimes was obtained by a change in
22 autocorrelation, itself linked to the lifetime of sunspots. In a second paper (Shapoval et al,
23 2014), we found additional evidence of the two regimes of the irregularity index using
24 embedding dimensions from 3 up to 32. During the first regime R1, from 1850 to 1915, λ
25 values were larger than during the second regime R2. The difference is most remarkably seen
26 at the minima of the Schwabe cycles. The value of λ at the recent minimum between cycles
27 23 and 24 was found to be as large as the largest value of λ prior to 1915, and much larger
28 than values between 1915 and 2000. This could signal a return of solar activity to regime R1.
29 In Shapoval et al (2014), we established that the two regimes of λ were stable with respect to
30 the parameters used in the computation and to de-trending (“de-cycling”) of the Schwabe
31 cycles.

1 In Shapoval et al (2013, 2014), we studied the two regimes of the irregularity index with
2 embedding dimension m between 3 and 16. In the present paper, we concentrate on the
3 smallest values of m (1 and 2). However our analysis cannot be performed at many solar
4 minima because the distances between nearby points in the phase space contain too many
5 zeros. Therefore, we first preprocess the data by smoothing them over $N=162, 324$ or 648
6 successive values (these numbers are chosen as multiples of 27 to suppress the influence of
7 solar rotation on the times series).

8 Several authors have suggested that observed solar (magnetic) time series are generated by an
9 (as yet) unknown low-dimensional dynamical system (see Zhang, 1996, and Sello, 2001, for a
10 review and original results). Attempts to reconstruct the dynamical system and to use it to
11 predict the future behavior of the time-series have led, **according to the reports of their**
12 **authors**, to reasonable medium-term predictions of the Schwabe cycle. The efficiency of
13 different predictions is out of the scope of this paper. **Pesnell's review (2012) of the prediction**
14 **of on-going cycle 24 together with Love & Rigler's (2012) and Choudhuri & Karak's (2012)**
15 **finding of random walk properties exhibited by some cycle-to-cycle characteristics constitute**
16 **a useful introduction to the subject. The horizon of the predictions based on chaotic models** is
17 linked to the estimates of Lyapunov exponents (Bershadskii, 2009; Zhang, 1996; Sello, 2001).
18 In these studies, Lyapunov exponents are focused on the low-frequency part of the data
19 spectrum, and the dynamical system is reconstructed based on at least decades of observation.
20 In the present paper, we use the irregularity index with embedding dimensions $m = 1$ and 2 to
21 characterize higher-frequency variations of *ISSN* in the period range of the QBO.

22 The next section (2) recalls the definition of the irregularity index and previous attempts to
23 use them in trying to characterize the solar dynamo. Section 3 illustrates further applications
24 of the irregularity index to the Wolf number *ISSN* and also to the geomagnetic index *aa*, with
25 results on the evolution of its higher frequency content. A simple autoregressive model is next
26 constructed in section 4, in order to try and reproduce some of the observed properties of the
27 irregularity index, and in particular the appearance (depending on the fundamental parameters
28 of the irregularity index and of model parameters) of half-Schwabe cycle peaks. The
29 discussion and conclusion are given in section 5.

1 2 Basic tools

2 This section recalls the definition of classical Lyapunov exponents and of the irregularity
3 index first introduced in Shapoval et al (2013). Further remarks that may be useful to better
4 appreciate the characteristics of the method are given in the Appendix.

5 2.1 Theoretical background

6 *Definition.* Lyapunov exponents are well defined for dynamical systems. Let F map a
7 m -dimensional Euclidian space Ω into itself. The Lyapunov exponent λ measures the rate of
8 exponential convergence or divergence of initially close points in a phase space under the
9 map F :

$$10 \quad \|J\varepsilon\| \sim \|\varepsilon\|e^\lambda, \quad \varepsilon \in \Omega$$

11 where J is the linear part (Jacobian matrix) of F , $\|\cdot\|$ is the norm in the phase space, and $\|\varepsilon\|$
12 is small.

13 Formally, we define the trajectory U_0, U_1, U_2, \dots

$$14 \quad U_1 = F(U_0), U_2 = F(U_1), \dots$$

15 for an arbitrary point U_0 of the phase space. The small distance ε_n in the neighborhood of U_n
16 becomes $\varepsilon_{n+1} = J(U_n)\varepsilon_n$ under the map F . Thus :

$$17 \quad \varepsilon_{n+1} = J_n \varepsilon_0, \quad J_n = J(U_n)J(U_{n-1})\dots J(U_0).$$

18 The limit :

$$19 \quad \lambda = \lim_{n \rightarrow \infty} \lim_{\varepsilon_0 \rightarrow 0} \frac{1}{n} \log \left(\frac{\|J_n \varepsilon_0\|}{\|\varepsilon_0\|} \right). \quad (1)$$

20 is the Lyapunov exponent. For so-called ergodic systems, limit (1) is the same for almost any
21 initial point U_0 (Oseledets, 1968; Eckmann and Ruelle, 1985).

1 *Reconstruction of a dynamical system.* Sometimes, when an underlying dynamical
 2 system does exist but is not known, a Lyapunov exponent can still be computed for a time
 3 series u_1, u_2, \dots, u_L , allowing one to reconstruct the key features of the dynamical system, i.e.
 4 the embedding dimension m and the map F (Wolf et al., 1985; Rosenstein et al., 1993; Kantz,
 5 1994). The vectors of the phase space are supposed to be:

$$6 \quad U_1 = (u_1, u_{T+1}, \dots, u_{(m-1)T+1}), \quad U_2 = (u_2, u_{T+2}, \dots, u_{(m-1)T+2}), \quad (2)$$

7 and so on, where T is a delay. The Lyapunov exponent is computed for the map F defined on
 8 the set $\{U_i\}$ by:

$$9 \quad F(U_n) = U_{n+1}. \quad (3)$$

10 A corollary of the fundamental Takens theorem (Takens, 1981) underlies this
 11 computation: let the time series be a projection of the orbit of a dynamical system that lies on
 12 its attractor \mathcal{A} and be dense on it. Then the Lyapunov exponents of the attractor \mathcal{A} and of the
 13 set $\{U_i\}$ are the same for an arbitrary delay T .

14 *Standard computational technique.* In practice, the time-series under study are always
 15 finite and noisy. Values of the delay T and of the embedding dimension m must first be
 16 selected in order to estimate the Lyapunov exponent. The delay is frequently taken to be the
 17 time of the first minimum of the autocorrelation function of the series, or that of its mutual
 18 information (Fraser and Swinney, 1986). The embedding dimension is chosen to be the
 19 minimal value m such that the map F transforms a neighborhood of each point U_i defined in
 20 (2) into a neighborhood of $F(U_i)$.

21 Given T and m , the Lyapunov exponent is to be inferred from the quantities:

$$22 \quad \log \left(\frac{\|J(U - V)\|}{\|U - V\|} \right) \quad (4)$$

23 for sufficiently close points U, V in the phase space Ω . Algorithms introduced by Rosenstein
 24 et al. (1993) and Kantz (1994) have been used with success in recent analyses of solar time
 25 series (Macek et al., 2006; Li and Li, 2007). In order to circumvent the rather slow

1 computation of the Jacobian, Ding and Li (2007) use the initial nonlinear map F rather than its
 2 linearization J when computing the ratio (4).

3 **2.2 Definition of the irregularity index**

4 **Based on the standard technique described in sections 2.1.2 and 2.1.3, this section**
 5 **introduces a straightforward definition of the quantity computed in the paper. In order to**
 6 **determine the irregularity index, we relax the requirement that close points in the phase space**
 7 **must be remote along the time axis, contrary to what is done for the Lyapunov exponent.**

8 **Phase space.** We consider a sliding window of L values u_1, u_2, \dots, u_L , where u_i is the i -
 9 th daily value of a given index, counted within the window. Given the embedding dimension
 10 m and delay T , define the vectors U_i in the phase space by (2).

11 **The map.** Let F be the displacement along the orbits given by (3).

12 **Nearest neighbors.** For each U_i , find the nearest point U_j which does not coincide with
 13 U_i . Specifically, take $j = \Psi(i)$ such that $\text{dist}(U_i, U_j) = \min_{U_l \neq U_i} \text{dist}(U_i, U_l)$, $l = 1, 2, \dots, L$; the
 14 distance between two vectors U_i and U_j is the square root of the sum of the squares of the
 15 differences between each vector coordinate $(\sum_{k=1}^m (u_{(k-1)T+j} - u_{(k-1)T+i})^2)^{1/2}$.

16 **Space-close points.** We next build the sequence Θ of the distances corresponding to the
 17 different¹ pairs $(U_i, U_{\Psi(i)})$, where i goes from 1 to L . Let $\tilde{L} = |\Theta|$ be the number of these pairs
 18 and d^* be the left α -quantile ($\alpha \in [0, 1]$) of Θ ; in other words, the pairs $(U_i, U_{\Psi(i)})$, $i \in \{1, \dots,$
 19 $L\}$ are ordered according to the distance between the two elements of each pair, so that the
 20 ordered sequence is $\{U_{i_k}, U_{\Psi(i_k)}\}$, $k = 1, \dots, \tilde{L}$, where $\text{dist}(U_{i_k}, U_{\Psi(i_k)}) \leq \text{dist}(U_{i_{k+1}}, U_{\Psi(i_{k+1})})$.
 21 P is defined as the first α -fraction of the ordered pairs, i.e. $P = \{(U_{i_k}, U_{\Psi(i_k)}) : k \leq \tilde{L} \alpha\}$.

22 **Small distances for formula (2).** We enlarge P to the set \tilde{P} by adding the pairs
 23 displaced along the orbit of each $(U_{i_k}, U_{\Psi(i_k)}) \in P$ until the distance between the elements in
 24 each pair becomes large enough (see below) or the end of the window is reached. Formally:

¹ If U_i is the nearest neighbor of U_j and U_j is the nearest neighbor of U_i then the distance $\text{dist}(U_i, U_j)$ is considered only once.

$$1 \quad \tilde{P} = \bigcup_{k=1}^{\tilde{L}} \{(U_{i_k}, U_{\Psi(i_k)}), (FU_{i_k}, FU_{\Psi(i_k)}), \dots, (F^l U_{i_k}, F^l U_{\Psi(i_k)})\}$$

2 such that (i) $\text{dist}(F^{l'} U_{i_k}, F^{l'} U_{\Psi(i_k)}) \leq d^*$, $l' = 0, 1, \dots, l$, (ii) either $l + i_k = L$ or $l + \Psi(i_k) = L$ (the
3 end of the window is reached) or $\text{dist}(F^{l+1} U_{i_k}, F^{l+1} U_{\Psi(i_k)}) > d^*$ (the distance is large enough).

4 **Irregularity index.** For each pair $(U, V) \in \tilde{P}$, we compute $\log [\text{dist}(FU, FV) / \text{dist}(U, V)]$
5 and define the irregularity index λ as the median of these numbers. The computed irregularity
6 index is assigned to the middle of the sliding window of length L . Let g be the lag between
7 two successive sliding windows (we use $g = L/8$, that is 6 months); we construct the new time
8 series:

$$9 \quad \lambda_{L/2}, \lambda_{L/2+g}, \lambda_{L/2+2g}, \dots$$

10 consisting of the irregularity indices found for sliding windows $[1, L]$, $[g + 1, g + L]$, $[2g + 1,$
11 $2g + L]$, and so forth. This new time series is considered as an additional solar index series.

12

13 **2.3 Some specifics of the irregularity index**

14 Many papers have aimed at reconstructing the dynamical system underlying long time-
15 series, such as the daily Wolf numbers (Spiegel and Wolf, 1987; Lawrence et al., 1995), the
16 monthly Wolf numbers (Ruzmaikin, et al., 1992; Price et al., 1992), and also some yearly
17 series (Ostryakov and Usoskin, 1990). These series are either sufficiently long (tens of
18 thousands of points for daily Wolf numbers) or smooth (since at least the 27-day variations
19 are averaged). The embedding dimension for these systems is generally taken to be at least 7,
20 and the delay T is of the order of months (see f.i. Greenkorn (2009) for a summary table).
21 However, smaller embedding dimensions ($4 < m < 9$) have been used by Greenkorn (2009)
22 for daily data over one Schwabe cycle. The latter paper shows that the Lyapunov exponent is
23 only weakly sensitive to the value of delay T as long as it remains small (a few days). The
24 orbit corresponding to the time series mentioned above now and then returns to the same
25 regions in the phase space. Usually, only points that are close in the phase space but far from
26 each other on the time axis are used to estimate the Lyapunov exponent (Rosenstein et al.,
27 1993).

1 In this paper, on the contrary, we do not set any limit to the distance in time of points
2 that are close in the phase space, and the exact definition of points being “close” is adapted to
3 the data being studied, using the ν -quantile of the smallest distances, as explained above.
4 When the embedding dimension $m = 1$, the smallest positive distance between two points in
5 the phase space is 1 because of the integer nature of *ISSN*. We find that at the minima of the
6 *ISSN* series many points lying at distance 1 are mapped along the corresponding trajectories to
7 points lying at exactly the same distance, so that the values of the irregularity index computed
8 at the signal minima can be inadequate (many values of the ratio (4) are zero). The transition
9 from $m = 1$ to $m = 2$ changes the properties of the exponent. Whereas we studied embedding
10 dimensions m from 4 to 6 in Shapoval et al (2013) and up to 32 in Shapoval et al (2014), we
11 concentrate here on the cases $m = 1$ and 2 that are the simplest, and because they shed light on
12 the occurrence of the quasi-biennial variations, at the focus of the present paper.

13 We first smooth the *ISSN* daily series and investigate the properties of the irregularity
14 index computed for different smoothings, with delay $T = 1$. We compute the irregularity index
15 within a 4-year sliding window: the choice of this 4yr length is a compromise between two
16 opposite requirements: first, the window must be sufficiently large to obtain a stable
17 determination of the irregularity index; second, it should be shorter than the Schwabe cycles.
18 We have checked that the values of the irregularity index calculated as explained are only
19 weakly sensitive to changes of window length inside a 3-5 year interval.

20

21 **3 Data analysis**

22 Solar activity is estimated in the paper with the Wolf (*ISSN*, sunspot) numbers, involving the
23 number of groups and the number of spots in each particular group. The number of groups
24 reflects the emerging magnetic field and is an indicator of activity. The number of spots
25 within a group depends on the magnetic field as such and also on the interaction between the
26 magnetic and velocity fields. In this paper, we mainly study sunspot numbers, but we also
27 present some preliminary results on Group Sunspot Numbers (Hoyt & Schatten, 1998) in
28 order to check that results are not affected by the way in which *ISSN* is determined (including
29 possible data heterogeneities).

1 The Wolf (sunspot) numbers (**International Sunspot Numbers, ISSN**) are defined as $K(10G +$
2 $s)$, where G is the number of sunspot groups, s is the number of individual spots, and K is a
3 factor that is relative to the observer. Daily data series of *ISSN* are available from 1849
4 onwards (**SIDC-team, 2005**). We now apply our algorithm to the *ISSN* series $w(t)$. **The time**
5 **series is strongly affected by the ~27-day signal connected to solar rotation and reflected axis**
6 **asymmetry of solar activity (Bartels 1934; Kitchatinov & Olemskoy, 2005; Howe 2009; Le**
7 **Mouël et al, 2007). Therefore the series is first smoothed in order to reduce the influence of**
8 **the Sun’s rotation.** Namely, it is averaged over multiples of 27 (days), i.e. $N = 162 (27 \times 6),$
9 $324 (27 \times 12),$ and $648 (27 \times 24)$ days. This results in new series $ISSN(t) = \sum_{k=t-[N/2]}^{t-[N/2]+N} w(k),$
10 where $[x]$ is the integer part of x .

11 *Case $m = 1$.* The evolution of the irregularity index λ computed with $m = 1$ and the three
12 values of N given above is shown (in blue) in **Figure 1**, together with the original *ISSN* series
13 smoothed over the same 4 year window (in red). With 162 day averaging (**Figure 1a**), there is
14 a clear one-to-one correspondence between Schwabe cycles of *ISSN* and λ . The maxima of the
15 cycles coincide precisely with each other in time. The λ “Schwabe cycles” exhibit asymmetry:
16 the rising segments are shorter and steeper than the decreasing ones. There is some structure
17 in the decreasing segments, sometimes in the form of a secondary maximum; minima in the
18 irregularity index cycles occur later than minima in the *ISSN* series.

19 When the data are smoothed over larger windows, oscillations with a period close to 5.5
20 years, i.e. half the period of the Schwabe cycle, appear (**Figure 1b, 1c**). We call these “*half-*
21 *Schwabe variations*” (HSV; see Shapoval et al, 2013, 2014). In the following, we use HSV to
22 refer to the presence of irregularity maxima at solar minima (thus generating a 5.5 year quasi-
23 periodicity), since the irregularity maxima at solar maxima are almost always present. We
24 also sometimes refer to HSV to refer to the amplitude or amplitude changes of the irregularity
25 peaks and their ratios (see below). In **Figure 1c**, both maxima and minima of the *ISSN*
26 Schwabe cycles correspond to maxima of HSV. Averaging over 324 days leads to an
27 intermediate behavior of the irregularity index (**Figure 1b**): secondary peaks at solar cycle
28 minima appear clearly in the 1870s and 1880s and after 1950, but some are not or hardly
29 visible at 1865, 1900 or 1975.

1 In order to provide a more quantitative measure of HSV behavior, we determine the ratio R of
2 the amplitude of λ -oscillations near maxima of $ISSN$ (Δ_{Smax}) to that near minima of $ISSN$
3 (δ_{Smin} ; $R = \delta_{Smin} / \Delta_{Smax}$ in Figure 2; the method is introduced in Shapoval et al (2013) and
4 further explained in the present paper). Figure 2 presents a schematic "Schwabe cycle"
5 (smoothed artificial signal in red; actually somewhat more than one full period) and its
6 irregularity index λ in blue. λ attains main maxima λ_{Smax} at the maxima of the (smoothed)
7 original signal, secondary maxima λ_{Smin} at the minima of the signal, and its minima λ_{mid} on the
8 descending and ascending phases of the signal (subscripts in this notation correspond to the
9 *signal* not to λ itself). Three local minima occur in Figure 2 (because somewhat more than one
10 cycle is represented) λ_{mid}^1 , λ_{mid}^2 , and λ_{mid}^3 . λ_{mid} is defined as their mean. Let
11 $\Delta_{Smax} = \lambda_{Smax} - \lambda_{mid}$ and $\delta_{Smin} = \lambda_{Smin} - \lambda_{mid}$. Δ_{Smax} and δ_{Smin} measure the amplitude of λ peaks
12 at signal maxima (minima) when they exist. Finally, $R = \delta_{Smin} / \Delta_{Smax}$ measures "HSV
13 performance", such that a decrease of R accompanies a clearer appearance of HSV.

14 The quantities λ_{Smax} , λ_{Smin} , and λ_{mid} can be determined even if the HSV structure is subdued.
15 λ_{Smin} is taken to be the *maximal* value of λ in a neighborhood of the *minimum* of the smoothed
16 original signal. We extend the construction of R to several solar cycles. In such a case the
17 quantities λ_{Smax} , λ_{Smin} , and λ_{mid} are obtained by averaging the corresponding quantities for all
18 cycles included in the time window of interest.

19 We see in Figure 1 that δ_{Smin} increases significantly (from ~ 0.1 to ~ 0.7) when N is increased
20 from 162 to 648 (HSV is actually hardly visible when $N = 162$ and almost as strong as peaks
21 at solar maxima when $N = 648$). This is mainly due to the large drop of λ_{Smin} as smoothing is
22 increased. In Figure 1b, we note differences in behavior between the period before and after
23 ~ 1930 (for instance lower overall mean value of λ and larger amplitude of HSV and Schwabe
24 cycles after 1930).

25 *Case $m = 2$.* The above computations are repeated for $m = 2$ (Figure 3). Different epochs can
26 readily be distinguished. First, both the amplitude of variations and actual values of λ change
27 around 1930, in a much more visible way than in the case $m = 1$, confirming that 1930 is a
28 time of first order regime change. This is particularly clear in Figure 3b where λ drops from a
29 mean value of about 0.3 to 0.2. This implies that the $ISSN$ -series becomes less irregular after
30 1930 (see discussion). In Figure 3a (162-day averaging), HSV is clearly visible in cycles 21 to

1 23, i.e. from 1975 onwards; it is still visible from about 1915 to 1975 but is barely
2 recognizable prior to 1915. 1915 and 1975 therefore appear as possible second order regime
3 changes or at least singularities. Increased smoothing strengthens HSV behavior. In **Figure**
4 **3b**, with 324-day averaging, HSV is seen with varying shapes and amplitudes from 1867 to
5 1930 and from 1945 to 2005, with a gap at the times of cycle minima 16-17 and 17-18. In
6 **Figure 3c**, with 648-day averaging, HSV is quite clearly present from 1867 to 1915, but it is
7 subdued from 1975 to 2005. We further note that some λ maxima at solar minima are
8 enhanced by increasing smoothing prior to 1915 (Cycles 12–13 and 13–14), whereas others
9 remain similar or are reduced after 1975 (Cycles 21-22 and 22-23).

10 Using the same notations as introduced for the case $m = 1$, we see (**Table 1a**) that indeed λ_{Smin}
11 is larger for the period 1867-1915 than for 1975-2008, both decreasing with increasing N , the
12 former from 0.37 to 0.22 and the latter from 0.30 to 0.10, when N increases from 162 to 648.
13 We see in **Figure 3** that HSV is better marked when N is increased for the period 1867-1915
14 and when N is decreased for the period 1975-2008. This can be expressed by the evolution of
15 the ratio $R = \delta_{Smin}/\Delta_{Smax}$ of the mean amplitudes of HSV peaks at solar minima vs solar
16 maxima as a function of N . When N increases from 162 to 648, this ratio increases from 0.67
17 to 0.79 for the period 1867-1915 but decreases from 0.71 to 0.34 for 1975-2008 (**Table 1a**).

18 In summary, the λ curves shown in **Figures 1** and **3** allow us to distinguish different epochs. In
19 **Figure 1**, we see the very strong appearance of HSV with an amplification of λ peaks at solar
20 cycle minima, and an indication of a change in behavior of δ_{Smin} values as a function of N
21 before and after ~ 1930 . In **Figure 3**, we also see that λ decreases in both mean value and
22 amplitude of variations in the 1930s. The R ratio increases with N for the period 1867-1915,
23 but it decreases in 1975-2008. So, evolution of the irregularity index reveals a first order
24 singular date ~ 1930 . Finer analysis of HSV properties (R-ratio evolution as a function of
25 smoothing) reveals second order singular dates around 1915 and 1975.

26

27 **4 A model**

28 We have already made a first attempt at constructing a model that would embody HSV
29 behavior of irregularity in solar activity as observed in real data in Shapoval et al (2013). We

1 extend here the method ,with slightly different choices of relevant parameters, to concentrate
2 on what could be related to the QBO.

3 **4.1 Definition of the model**

4 Consider a first order autoregressive AR(1) process $x(t)$:

$$5 \quad x(t) = ax(t-1) + \eta(t),$$

6 where the random variable $\eta(t)$ is Poissonian with mean $\mu(t)$, $P\{\eta = n\} = e^{-\mu} \mu^n / n!$. The mean
7 $\mu(t)$ is modulated by the sum of two periodic functions (as opposed to only one in Shapoval et
8 al, 2013) with periods T_1 and T_2 , $T_1 > T_2$. The longer period T_1 is set to 11 years (11×365
9 days), corresponding to the Schwabe cycle. We choose the shorter (which we call
10 intermediate) period T_2 in the range from 1 to 3 years, such that it includes the QBO. So :

$$11 \quad \mu(t) = h \left(-\cos \frac{2\pi t}{T_1} - k \cos \frac{2\pi t}{T_2} + c \right), \quad (5)$$

12 where $h > 0$, $0 < k < 1$; $c > 1 + k$ is a vertical shift. The synthetic signal $w(t)$ is defined by

$$13 \quad w(t) = [Mx(t)], \quad (6)$$

14 M is set to 10 to mimic the factor in the definition of the group sunspot number. This yields
15 the same order of magnitude for synthetic and observed *ISSN* values.

16 The model is a function of variable t (time, in days) and depends on five adjustable
17 parameters: a , h , T_2 , k and c . The value of parameter a in the auto-regressive process
18 determines the correlation of the data. Modeling the sunspot series by an autoregressive
19 AR(1) model connects a to the lifetime of sunspots (Blanter et al., 2005). h controls the
20 smoothness of the signal. The factor $k < 1$ controls the relative amplitude of the T_2 vs T_1
21 modulations. The vertical shift c controls the ratio of the maximum to the minimum of λ .
22 Figure 4 shows an example of a realization of the model with parameters given in the legend.

23

1 4.2 Modeling results

2 *Appearance of HSV with data smoothing (case $m = 1$).* Already with $m = 1$ and without
3 intermediate period modulation T_2 ($k = 0$), HSV appears in response to increasing data
4 smoothing (Figure 5). For $N = 162$ days, λ shows no HSV maxima at solar minima. When N
5 is increased to 648, all λ values decrease, but their overall structure changes markedly. λ
6 remains approximately the same at solar minima, decreases slightly at solar maxima and falls
7 dramatically in intermediate intervals (corresponding to the ascending and descending phases
8 of the “solar” cycle). As a result, λ now peaks sharply not only at solar maxima but also at
9 solar minima: this behavior is indeed reminiscent of that observed for *ISSN* (compare Figures
10 5 and 1a and 1c), as looked for when building the model.

11 *Increase in HSV behavior as a function of data smoothing (case $m = 2$).* The behavior of the
12 irregularity index for $m = 2$ is significantly richer. We set intermediate period variations at a
13 relatively strong level ($k = 0.35$, Figure 6): the irregularity index exhibits HSV that increases
14 as smoothing is increased (see Figure 6a to 6c when averaging interval goes from 162 days -
15 solid gray lines - to 648 days - dashed black lines). In the case when $T_2 = 610$, $N = 648$, strong
16 HSV peaks are always present except in 1 out of 10 possible occurrences (at $y = 11$, Figure
17 6b). On the contrary, for the same T_2 but with $N = 162$, HSV peaks are quite subdued (yet
18 generally visible), though again only 1 out of 10 is missing (at $y = 41$, Figure 6b). In that case,
19 increasing data smoothing in the model results in amplifying HSV behavior: R increases from
20 0.39 to 0.56 (Table 1b). HSV increases (that is R increases) with smoothing when T_2 is in the
21 interval [450, 700]; Figure 6a to 6c). The effect slowly disappears when T_2 reaches 800
22 (Figure 6d).

23 Figure 7 illustrates the effect of changing the value of the “vertical shift” c when there is no
24 intermediate period modulation ($k = 0$). HSV behavior becomes increasingly significant as c
25 is increased: R grows from ~ 0.1 to 0.8 as c increases from 1.2 to 1.7 (Table 1c).

26 Comparing Figure 6c (where $k = 0.35$) with Figure 7d (where $k = 0$; $a = 0.8$, $h = 0.4$, $c = 1.7$ in
27 both cases), we see that HSV behavior is more visible in the case of a smaller N (162) when k
28 is smaller (R is then respectively 0.31 vs 0.77, Table 1c). When $k = 0$, there is little or no HSV
29 increase (R increases from 0.77 to 0.83, Table 1c, and Figure 7b, 7c, 7d) whereas with $k =$

1 0.35 it grows significantly (from 0.31 to 0.70, Table 1b). Therefore, k is an important factor
2 controlling HSV behavior.

3 *Decrease of HSV as a function of data smoothing (case $m = 2$).* When intermediate period
4 (T_2) variations are suppressed and parameter h (that controls the smoothness of the signal) is
5 increased (Figure 8), we find another regime in which HSV decreases with increasing
6 smoothing. When N increases from 162 to 648, the R ratio decreases from 0.69 to 0.43 (Table
7 1d).

8 *A direct comparison of model with observations.* In Figure 9, we model the data of cycles 21
9 to 23 (which have similar durations, to allow a comparison with a model where $T_1 = 11$
10 years). **Parameter k is set to zero and a to 0.9. This choice of a reflects the increase of the**
11 **lifetime of sunspots found by Blanter et al (2005).** We can now directly compare the
12 irregularity index computed for the synthetic and actual signals.

13 Since the model contains a random ingredient and the computation of the irregularity index is
14 sensitive to particular realizations, two of them are shown in Figure 9. The irregularity index
15 for the model follows rather precisely that for *ISSN* for $N = 162$ (Figure 9, middle row, except
16 at the minimum between cycles 22 and 23 in the realization on the right side). The quality of
17 the fit is somewhat less for $N = 648$ (Figure 9, bottom row). Nevertheless, the model
18 realizations globally reproduce the λ pattern of the real data quite faithfully.

19 An explicit comparison (Figure 9) of the irregularity index for the model and *ISSN* time series
20 is possible for cycles 21-23 (1975-2005) because λ constructed with *ISSN* exhibits a smooth,
21 quasi-cyclic and regular behavior, as is the case for model realizations. The regime observed
22 in 1867-1915 does not display such regular cycles of λ and therefore does not allow such an
23 easy comparison.

24

25 **5 Summary, discussion and conclusion**

26 The evolution of the daily values of sunspot number *ISSN* from 1850 to 2005 has been studied
27 in this paper, using tools from dynamical systems. Some interesting results are obtained with
28 the irregularity index, a new method introduced in Shapoval et al (2013, 2014). The method

1 computes the rate of divergence of close trajectories in the phase space under a one-step
2 translation mapping. This index is akin to the maximal Lyapunov exponent for time series
3 calculated for low-dimensional dynamical systems, but is applicable to short time series with
4 a random component. We have computed the irregularity index λ of *ISSN* for embedding
5 dimensions $m = 1$ and 2 within a 4-year sliding window, after first averaging the data over N
6 $= 162, 324$ and 648 days (multiples of the solar rotation period). The irregularity index for N
7 $= 162$ follows Schwabe cycle (Figure 1), with sharp, high peaks at solar cycle maxima. But
8 when N becomes large enough, it also exhibits sharp maxima at solar cycle minima (see also
9 Shapoval et al, 2013), resulting in 5.5-year time variations, i.e. half the period of the Schwabe
10 cycles (Figure 1 middle and bottom, Figure 3); we call them *half-Schwabe variations* (HSV).

11 The mean level of the irregularity index for *ISSN* undergoes a downward step around 1930
12 (particularly clear with embedding dimension $m=2$, as seen in Figure 3). This can be linked to
13 the observation by Bershadskii (2008) that a change in the fractal properties of *ISSN* took
14 place at that time. For a given time period, HSV can be characterized by the mean differences
15 δ_{Smin} of λ values at the times of Schwabe cycle minima (λ_{Smin}) and the mean of λ minima (λ_{min})
16 at the middle times of the descending and ascending phases of the Schwabe cycles; we use the
17 ratio R of δ_{Smin} over its equivalent δ_{Smax} taken at the times of Schwabe cycle maxima. A first
18 regime (denoted by Q1) is characterized by R increasing with N , and a second one (Q2) has R
19 decreasing with N . For *ISSN*, with $m = 2$, Q1 is observed until ~ 1915 , whereas Q2 appears
20 after ~ 1975 ; the main transition may be around 1930 (Figure 3).

21 HSV as such may not be regarded as a result with great importance. Our functional λ can
22 attain its extrema on both ascending and descending phases. If such is the case, HSV appears
23 because of a certain similarity between these ascending and descending phases. That is why
24 we cannot yet discuss the physics underlying the essence of HSV. On the other hand, we are
25 entitled to look for simple time series that would display the properties observed for *ISSN*.

26 A synthetic signal, generated by a simple autoregressive model of order 1, exhibits many of
27 the above-mentioned properties of the irregularity index of *ISSN*. The random part of this
28 synthetic signal is taken to be Poissonian. Its mean is modulated by the sum of two periodic
29 functions with periods $T_1 = 11$ years and $T_2 < T_1$, the latter being tunable in an interval that
30 can range from months to years. The introduction of intermediate oscillations (T_2) allows one
31 to reproduce both the Q1 as well as the Q2 regime (Table 1). When the embedding dimension

1 m is 1, HSV (5.5 year pseudo-period) oscillations appear even if T_2 variations are absent ($k=0$;
2 Figure 5). When m is equal to 2, the behavior of the irregularity index series becomes richer:
3 regime Q1, in which HSV behavior increases with smoothing N , is observed for larger values
4 of k (Figure 6), whereas regime Q2, in which HSV decreases with N , is obtained when
5 intermediate period (T_2) variations are absent ($k = 0$) and parameter h (that controls the
6 smoothness of the signal) is increased (Figure 8). We conclude that high frequency
7 components of *ISSN* have much in common with an AR(1) process. The presence and then
8 disappearance of ~ 1 -2 year (T_2) oscillations seem to be required to produce a transition
9 between regimes Q1 and Q2 (when $m = 2$). We propose that these oscillations may be linked
10 to the QBO, the second most powerful solar variation after the 11-yr cycle (e.g. Ivanov et al.,
11 2002).

12 At first order, the observed change in the mean level of λ around 1930 found in this paper
13 could mark a shift of solar activity to a new regime (a transition of the solar dynamical system
14 to a new state). This regime change is also marked by a (second order) change in the way
15 HSV amplitude varies as the data is increasingly smoothed. These observed features can be
16 reproduced by the model: the R ratio increases with increasing N (Q1) prior to 1915 and
17 decreases after 1975 (Q2). **Although several model parameters interact to promote one or the
18 other regime, the most important one appears to be parameter k that reflects the presence or
19 absence of intermediate T_2 variations in the process. The shift of the irregularity index of *ISSN*
20 from regime Q1 to Q2 may be due to the decrease or even disappearance of QBO.**

21 **In contrast to a standard statistical analysis, one cannot introduce a reasonable null hypothesis
22 in the present study. Instead, we have checked the stability of the observed phenomena with
23 respect to the parameters that control the irregularity index and we have tested the
24 significance of our conclusions with the auto-regressive model.**

25 The homogeneity of the *ISSN*-series is a long debated question. Svalgaard (2010, 2012)
26 points to an abrupt increase of *ISSN* in ~ 1945 and argues that this increase is caused by
27 changes in the measurement rules. The NASA web-site
28 (<http://solarscience.msfc.nasa.gov/greenwch.shtml>) also notes that the sunspot series is not
29 uniform; abrupt changes occurred in 1941-1942 (sunspot numbers) and 1976-1977 (**sunspot
30 areas, not used in our paper**). **However, our conclusions about regime changes are not**

1 seriously affected by such events, because we use ratios (equation 4). Moreover, the date of
2 the ~1930 singularity is remote from 1941-1942 (or 1945).

3 In order to see whether the observed behavior of the irregularity index of *ISSN* could be
4 affected by such data problems, we have computed the irregularity index for another proxy
5 influenced by solar activity but derived completely independently, namely the geomagnetic
6 index *aa* (available at <http://isgi.latmos.ipsl.fr/source/indices/aa/>). With $m = 1$, we computed
7 the irregularity index for *aa* as such (without any prior averaging over multiples of 27 days).
8 The values of $\lambda(t)$ (Figure 10) exhibit both a noticeable increase in mean level (from about
9 1.75 to 2) and a decrease in range (from 0.5 to 0.2) in the 1930s. The sign of the change in
10 mean value is opposite to that found for the irregularity index of *ISSN* (Figure 10 vs Figure 3),
11 but the same singularity in solar behavior could be at the origin of both.

12 Although this paper focuses mainly on changes of the irregularity index with smoothing, we
13 also describe briefly changes of λ with time, in order to provide further evidence of the
14 robustness of the technique. Our previous paper (Shapoval et al, 2013) examines the time
15 evolution of λ computed for *ISSN* with a 4-year sliding window and different embedding
16 dimensions and finds a change of regime in approximately 1915-1940. The same computation
17 has been repeated for the Hoyt and Schatten group sunspot numbers (GSN, Hoyt & Schatten,
18 1998). Despite differences in inhomogeneities and potential problems with the two series, the
19 main results are quite similar, excluding the possibility of an artefact due to the choice of an
20 imperfect time series. The irregularity index of GSN exhibits two different regimes with a
21 clear transition in the period 1915-1940 (details and Figures in Appendix B). This strengthens
22 the result obtained for *ISSN* and published in Shapoval et al (2013) and further supports our
23 approach, as used in the present paper.

24 It would be good to find some physical evidence to support our hypothesis that the change of
25 regime can be linked to QBO rarefactions. There has been a significant amount of research on
26 oscillations in the 1-2 year period range in cosmic rays (Valdes-Galicia et al., 1996; Kudela et
27 al., 2002; Rouillard and Lockwood, 2004) and in mid-latitude coronal holes area (McIntosh et
28 al., 1992). Obridko and Shelting (2007) give a brief review of these works, together with new
29 results (see also f.i. Ivanov et al., 2002). Intermediate variations do not seem to have been
30 reported up to now for *ISSN*, but further interesting observations have been made for *aa*
31 (Lockwood, 2001; Mursula et al., 2003). Using an extended *aa* index over 160 years, Mursula

1 et al. (2003) have found that the power of “mid-term quasi-periodicities” (identical to QBO)
2 is larger at periods alternating between 1.3 and 1.6 years; maxima of 1.3-year oscillations
3 occur at the maxima of Schwabe cycles 18 and 22, while the 1.6-yr oscillations peak at the
4 maxima of cycles 16 and 21. Spectral power of *aa* is high during periods of high solar activity
5 and would reflect the strength of the solar dynamo. Sudden disappearance of power is
6 considered as a precursor for long-term decreases in solar activity. Our observations of a post-
7 1975 decrease of *R* ratio with smoothing and our modeling of this regime by using an AR(1)
8 process without T_2 -variations are in line with the work of Mursula et al. (2003).

9 At least two different mechanisms could generate QBO. On one hand, Ivanov et al. (2002)
10 show that the QBO of solar magnetic fields are mainly revealed in their large-scale
11 component; they argue that QBO actually reflect variations in the equatorial dipole (and to a
12 lesser extent quadrupole); for these authors, QBO sources are located near the base of the
13 convection zone and remain invariable. Vecchio et al. (2012), using magnetic synoptic maps
14 from 1976 to 2003, propose that QBO are fundamental modes associated with poleward
15 magnetic flux migration from low to high latitudes (part of meridional circulation) during the
16 maximum and descending phases of the solar cycle. A strong link between QBO and the solar
17 dynamo is inferred from these and other works. Time variations of QBO might therefore
18 provide information on changes in meridional flow. On the other hand, non-linearity of the
19 solar dynamo itself could be the source of QBO. Using a non-linear Babcock-Leighton model,
20 Charbonneau et al. (2007) support the hypothesis that the non-linear component of the solar
21 dynamo prevails over the stochastic one. Mayr and Schatten (2012) argue that the strong non-
22 linearity in the Charbonneau et al. equations could generate QBO without any time-dependent
23 solar excitation.

24 ~~HSV behavior of the irregularity index of *ISSN* could be related to strong QBO before 1915-~~
25 ~~1930 and strong decrease afterwards, notably after 1975, possibly corresponding to an~~
26 ~~important change in the regime of solar activity.~~ The irregularity index of *ISSN* computed in
27 this paper may provide a measure of the irregular behavior of the solar dynamo. Duhau and de
28 Jager (2008) propose that *ISSN* may be used as a proxy of the toroidal component of the
29 Sun’s magnetic field and *aa* of the poloidal component. The irregularity index of *aa* as such
30 presents a change in the 1930s, with a sign opposite to that for *ISSN*. We could therefore
31 interpret our observations of changes in regime of the irregularity indices of *ISSN* and *aa* as
32 indicating respectively a decrease in the irregular character of the toroidal field and an

1 increase in the irregularity of the poloidal field in the 1930s, date of the advent of a Grand
2 Maximum period in solar activity. Our analysis also suggests that another change may have
3 started around 1975, as witnessed by decreasing HSV as a function of smoothing (see Figures
4 3a to 3c in that order). This may have heralded the 2005 change found in our complementary
5 studies of the irregularity index (Shapoval et al, 2013, Figure 2 to 5; Shapoval et al, 2014,
6 Figures 1 to 3).

7 The irregularity index method is promising but still not a fully understood tool. It appears to
8 be able to uncover singular phenomena and solar activity changes that cannot easily be seen
9 by other means, but the tool depends on a number of parameters, particularly the embedding
10 dimension and changes of behavior as the embedding dimension is changed. We note that the
11 regime changes R1 and R2 uncovered by Shapoval et al (2013, 2014) are not identical to the
12 regime changes Q1 and Q2 found in the present paper. The R1/R2 regimes are marked by
13 different levels of the irregularity index (computed with embedding dimensions from 4 to 32).
14 In the present paper, when embedding dimension m is 2, we also find some evidence of the
15 R1/R2 regimes (Figure 3a and b). But we introduce an additional tool, the analysis of the
16 irregularity index as a function of data smoothing (N), and this is what reveals the Q1/Q2
17 regimes. Although R1 and Q1, ending around 1915-1930, could correspond to the same
18 regime, R2 (starting after 1930 and possibly ending in 2008) and Q2 (emerging clearly only
19 after 1975) do not coincide. The physical nature of these singularities and the differences in
20 their timing and behavior remain to be deciphered.

21

22 **Appendix A: Examples of computation of the irregularity index**

23 In order to illustrate some aspects of the computations involved in this paper, we
24 generate synthetic data with the formula :

$$25 \quad u(t) = \sin \frac{2\pi t}{20} + \eta(t), \quad t = 1, 2, \dots, 19,$$

26 where $\eta(t)$ is a random variable uniformly distributed over $[-0.05, 0.05]$. The
27 embedding space is one-dimensional ($m = 1$).

28 Figure 11 exhibits 19 points of the sample. For each point, we first find the nearest
29 neighbor. In the present case, only 13 pairs of nearest neighbors are different, so that the set of
30 distances consists of 13 values. Let $\nu = 0.25$. Since the integer part of $0.25 \cdot 13$ is 3, the ν -

1 quantile d^* is the third distance from the lowest one. Distances less than or equal to d^* are
2 “small”, according to our definition. For each pair of nearest neighbors, the map F defined in
3 equation (3) that moves points along their trajectory is applied, the distance between the
4 corresponding images being small. In the example above the pair at times 6 and 19 (red points
5 in Figure 11) possesses the smallest distance. A move to the right is impossible because 19 is
6 the largest time in the window. Thus, this pair does not contribute to the computation of the
7 exponent.

8 The points at times 4 and 11 form the next pair (blue filled circles). The distance
9 between $u(5)$ and $u(12)$ (blue empty circles), which is $|u(12) - u(5)|$, is larger than d^* ,
10 therefore this pair generates a single quantity $\log [|u(12) - u(5)| / |u(11) - u(4)|]$ as a candidate
11 irregularity index.

12 The last pair under consideration is $[u(1), u(11)]$. Since the value $u(11)$ appears twice
13 in the pairs we consider, the corresponding point in the graph is marked first by a blue circle
14 and second by a green circle (the green circle is smaller). Although the values $u(2)$ and $u(12)$
15 are very close, the distance between $F(u(1)) = u(2)$ and $F(u(11)) = u(12)$ is larger than the
16 critical distance. Thus, the quantity $\log [|u(12) - u(2)| / |u(11) - u(1)|]$ becomes the second
17 candidate to the irregularity index. The irregularity index is chosen as the median of the
18 candidate values.

19

20 **Appendix B. Regime change of λ of GSN and ISSN.**

21 The irregularity index λ of both ISSN and GSN is computed with a 4-year sliding
22 window, 8-day delay, and embedding dimensions 2-32. According to Figures 12 and 13, λ of
23 both the series exhibits two different patterns before ~1915 and after ~1940 with a transition
24 during 1915-1940. The patterns for ISSN differ by the values of the irregularity index. High
25 values of the irregularity index, most markedly seen at the minimum of cycles 14-15, underlie
26 the pattern prior to 1915. The second pattern continues with the minimum of cycles 23-24
27 when λ achieves another remarkable maximum.

28 The irregularity index of GSN also exhibits 4 high maxima at the minima of cycles 11-
29 15. We cannot check existence of the cycle 23-24 peak since recent data, following the Hoyt
30 and Schatten technique, are not available as open sources. This confirmation of the regime
31 change of solar activity between 1915 and 1940 vindicates our approach and results.

1

2 **Acknowledgements**

3 IPGP provided support to A. Shapoval and M. Shnirman during their visit to the institute. A.
4 Shapoval was partially supported by RFBR grants 14-01-00346 and 14-01-00773. IPGP
5 contribution NS xxx (to be written when available).

6

1 **References**

- 2 Bartels, J.: 1934, Twenty-Seven Day Recurrences in Terrestrial-Magnetic and Solar Activity,
3 1923-1933, *Terrestrial Magnetism and Atmospheric Electricity* 39, 201–202.
- 4 Bergé, P., Pomeau, Y., Vidal, C.: 1984, *L'Ordre dans le Chaos*, Hermann, Paris, France, 353
5 pp.
- 6 Bershadskii, A.: 2008, New dynamics of the Sun convection zone and global warming.
7 arXiv:0805.2108v1 [astro-ph.SR].
- 8 Bershadskii, A.: 2009, Chaotic mean wind in turbulent thermal convection and long-term
9 correlations in solar activity, . arXiv:0908.4008v4 [astro-ph.SR]].
- 10 Blanter, E.M., Shnirman, M.G., Le Mouél, J.-L.: 2005, Solar variability: Evolution of
11 correlation properties. *J. Atmos. Solar-Terr. Phys.* 67, 521 – 534.
- 12 Blanter, E.M., Le Mouél, J.-L., Perrier, F., Shnirman, M.G.: 2006, Short-term correlation of
13 solar activity and sunspot: evidence of lifetime increase. *Solar Phys.* 237, 329 – 350.
- 14 Charbonneau, P., Beaubien, G., St-Jean, C.: 2007, Fluctuations in Babcock-Leighton dynamo:
15 II. Revisiting the Gnevyshev-Ohl rule. *The Astrophysical Journal* 658, 657 – 662.
- 16 Choudhuri, A.R., and Karak, B.B., 2012, Origin of Grand Minima in Sunspot Cycles, *PRL*,
17 109, 171103 – 171106.
- 18 Ding, R., Li, J.: 2007, Nonlinear finite-time Lyapunov exponent and predictability. *Physics*
19 *Letters A* 364, 396 – 400.
- 20 Duhau, S., de Jager, C.: 2008, The Solar Dynamo and its Phase Transitions during the Last
21 Millenium. *Solar Phys.* 250, 1 – 15.
- 22 Eckmann, J.-P., Ruelle, D.: 1985, Ergodic theory of chaos and strange attractors. *Reviews of*
23 *Modern Physics* 57, 617 – 656.
- 24 Fraser, A.M., Swinney, H.L.: 1986, Independent coordinates for strange attractors from
25 mutual information. *Phys. Rev. A* 33, 1134 – 1140.
- 26 Greenkorn, R.A.: 2009, Analysis of Sunspot Activity Cycles. *Solar Phys.* 255, 301 – 323.
27 doi:10.1007/s11207-009-9331-z.
- 28 Howe R. 2009, Solar interior rotation and its variation. *Living Rev. Solar Phys.* 6, 1 – 91.

- 1 Hoyt, D. V. and Schatten, K. H., 1998., Group Sunspot Numbers: A new Solar Activity
2 Reconstruction, in *Solar Physics*, V. 181, 491-512.
- 3 Ivanov, E.V., Obridko, V.N., Shelting, B.D.: 2002, Quasi-biennial oscillations of the solar
4 magnetic fields. In: Wilson, A. (ed.) *Solar variability: from core to outer frontiers*. The 10th
5 European Solar Physics Meeting, 9–14 September 2002, Prague, Czech Republic, ESA SP-
6 506 v. 2, ESA Publications Division, ISBN 92-9092-816-6, Noordwijk, 847 – 850.
- 7 Kantz, H.: 1994, A robust method to estimate the maximal Lyapunov exponent of a time
8 series. *Physics Letters A* 185, 77 – 87.
- 9 Kitchatinov, L.L., Olemskoi, S.V.:2005, Active longitudes of the sun: The rotation period and
10 statistical significance, *Astronomy Letters*, 31, 280 – 284.
- 11 Kudela, K., Rybak, J., Antalova, A., Storini, M.: 2002, Time evolution of low-frequency
12 periodicities in cosmic ray intensity. *Solar Phys.* 205, 165 – 175.
- 13 Lawrence, J.K., Cadavid, A.C., Ruzmaikin, A.A.: 1995, Turbulent and chaotic dynamics
14 underlying solar magnetic variability. *Astron. Astrophys.* 455, 366 – 375.
- 15 Lawrence, J.K., Cadavid, A.C., Ruzmaikin, A.A.: 2008, Rotational Quasi-Periodicities and
16 the Sun-Heliosphere Connection. *Solar Phys.* 252, 179 – 193.
- 17 Le Mouél, J.-L., Shnirman, M.G., Blanter, E.M.: 2007, The 27-Day Signal in Sunspot
18 Number Series and the Solar Dynamo. *Solar Phys.* 246, 295 – 307.
- 19 Li, Q.-X., Li, K.-J.: 2007, Low dimensional chaos from the group sunspot numbers. *Chinese*
20 *Journal of Astronomy and Astrophysics* 7, 435 – 440.
- 21 Lockwood, M.: 2001, Long-term variations in the magnetic fields of the sun and the
22 heliosphere: their origin, effects and implications. *J. Geophys. Res.* 106, 16021 – 16038.
- 23 Love, J.J., Rigler, E.J, 2012, Sunspot random walk and 22-year variation, *GRL*, 39, L10103 –
24 L10108.
- 25 Macek, W.M., Bruno, R., Consolini, G.: 2006, Testing for multifractality of the slow solar
26 wind. *Adv. Space Res.* 37, 461 – 466.
- 27 Mavromichalaki, H., Preka-Papadema, P., Petropoulos, B., Tsagouri, I., Georgakopoulos, S.,
28 Polygian, J.: 2003, Low- and high-frequency spectral behavior of cosmic-ray intensity for the
29 period 1953–1996. *Annales Geophysicae* 21, 1681 – 1689.

- 1 Mayr, H.G., Schatten, K.H.: 2012, Nonlinear oscillators in space physics. *Journal of*
2 *Atmospheric and Solar-Terrestrial Physics* 74, 44 – 50.
- 3 McIntosh, P.S., Thompson, R.J., Willock, E.C.: 1992, A 600-day periodicity in solar coronal
4 holes. *Nature* 360, 322 – 324.
- 5 Mursula, K., Zieger, B., Vilppola, J.H.: 2003, Mid-term quasi-periodicities in geomagnetic
6 activity during the last 15 solar cycles: connection to solar dynamo strength. *Solar Phys.* 212,
7 201 – 207.
- 8 Obridko, V.N., Shelting, B.D.: 2007, Occurrence of the 1.3-year periodicity in the large-scale
9 solar magnetic field for 8 solar cycles. *Adv. Space Res.* 40, 1006 – 1014.
- 10 Oseledets, V.I.: 1968, A multiplicative ergodic theorem. Lyapunov characteristic numbers for
11 dynamical systems. *Trans. Moscow Math. Soc.* 19, 197 – 231.
- 12 Ostryakov, V.N., Usoskin, I.G.: 1990, On the dimension of solar attractor. *Solar Phys.* 127,
13 405 – 412.
- 14 **Pesnell, W.D., 2012, Solar Cycle Predictions (Invited Review), *Solar Phys.*, 281, 507-532.**
- 15 Price, C.P., Prichard, D., Hogenson, E.A.: 1992, Do the sunspot numbers form a chaotic set?
16 *J. Geophysical Research* 97, 19113 – 19120.
- 17 Rosenstein, M.T., Collings, J.J., De Luca, C.J.: 1993, A practical method for calculating
18 largest Lyapunov exponents from small data sets. *Physica D* 65, 117 – 134.
- 19 Rouillard, A., Lockwood, M.: 2004, Oscillations in the open solar magnetic flux with a period
20 of 1.68 years: imprint on galactic cosmic rays and implications for heliospheric shielding.
21 *Annales Geophysicae* 22, 4381 – 4385.
- 22 Ruzmaikin, A., Feynman, J., Kosacheva, V.: 1992, On Long-Term Dynamics of the Solar
23 Cycle. In: Harvey, K.L. (ed.) *The solar cycle; Proceedings of the National Solar*
24 *Observatory/Sacramento Peak 12th Summer Workshop* 27, ASP Conference Series, San
25 Francisco, 547 – 556.
- 26 Sello, S.: 2001, Solar cycle forecasting: A nonlinear dynamics approach. *Astron. Astrophys.*
27 377, 312 – 320.
- 28 Shapoval, A., Le Mouél, J.-L., Courtillot, V., Shnirman, M.: 2013, Two regimes in the
29 regularity of sunspot numbers, *The Astrophysical Journal*, 779, 108 – 116.

1 Shapoval, A., Le Mouél, J.-L., Courtillot, V., Shnirman, M.: 2014, submitted, Is a sudden
2 increase of irregularity of sunspot numbers a precursor of a return to low solar activity?, J.
3 Geophys. Res.

4 SIDC-team, World Data Center for the Sunspot Index, Royal Observatory of Belgium,
5 *Monthly Report on the International Sunspot Number*, online catalogue of the sunspot index:
6 <http://www.sidc.be/sunspot-data/>, '1850-2005'.

7 Spiegel, E.A., Wolf, A.: 1987, Chaos and the Solar Cycle. In: Buchier, J.-R., Eichhorn, H.
8 (eds.) *Chaotic Phenomena in Astrophysics*, Ann. N.Y. Acad. Sci., New York, 55.

9 Svalgaard, L., 2010, Updating the Historical Sunspot Record, arXiv:1003.4666 [astro-ph.SR].

10 Svalgaard, L., 2012. How well do we know the sunspot number? Comparative Magnetic
11 Minima: Characterizing quiet times in the Sun and Stars. Proceedings of the International
12 Astronomical Union, IAU Symposium 286, 27-33.

13 Takens, F.: 1981, In: Rand, D.A., Young, L.S. (eds.) *Detecting strange attractors in*
14 *turbulence*, Springer, Berlin, 366 – 381.

15 Valdes-Galicia, J.F., Perez-Enrriquez, R., Otaola, J.A.: 1996, The cosmic ray 1.68 year
16 variation: a clue to understand the nature of the solar cycle? *Solar Phys.* 167, 409 – 417.

17 Van der Linden, R.A.M., SIDC team: 2005, Online catalogue of the sunspot index.

18 Vecchio, A., Laurenza, M., Carbone, V., Storini, M.: 2010, Quasi-biennial modulation of
19 solar neutrino flux and solar and galactic cosmic rays by solar cyclic activity. *The*
20 *Astrophysical Journal Letters* 709, L1 – L5.

21 Vecchio, A., Laurenza, M., Meduri, D., Carbone, V., Storini, M.: 2012, The dynamics of the
22 solar magnetic field: polarity reversals, butterfly diagrams, and quasi-biennial oscillations.
23 *The Astrophysical Journal* 749, 27 – 36. doi:10.1088/0004-637X/749/1/27.

24 Wolf, A., Swift, J.B., Swinney, H.L., Vastano, J.A.: 1985, Determining Lyapunov Exponent
25 from a Time Series. *Physica D* 16, 285 – 317.

26 Zhang, Q.: 1996, A nonlinear prediction of the smoothed monthly sunspot numbers. *Astron.*
27 *Astrophys.* 310, 646 – 650.

28

1 Table 1. Calculation of R ratio values (see text). N is the number of days over which the *ISSN*
2 data are smoothed to remove in particular the effect of solar rotation; λ_{Smin} is the mean value
3 of the maxima of the irregularity index at the times of solar minima over the period range
4 indicated under the heading “years” (by default 1867-2008 when not indicated); λ_{Smax} is the
5 mean value of the maxima of the irregularity index at the times of solar maxima over the
6 same period range; λ_{min} is the mean value of the minima of the irregularity index as indicated
7 in note 2 in the text; $\delta_{Smin} = \lambda_{Smin} - \lambda_{min}$; $\Delta_{Smax} = \lambda_{Smax} - \lambda_{min}$; $R = \delta_{Smin} / \Delta_{Smax}$. Each part of the
8 Table corresponds to a Figure as indicated.

9 Table 1a (corresponding to Figure 3)

10

11	N	λ_{Smin}	λ_{Smax}	λ_{min}	δ_{Smin}	Δ_{Smax}	R	years
13	162	0.37	0.43	0.23	0.14	0.20	0.67	1867-1910
14	324	0.31	0.35	0.15	0.16	0.19	0.83	
15	648	0.22	0.25	0.10	0.12	0.15	0.79	
16								
17	162	0.30	0.34	0.18	0.12	0.17	0.71	1970-2008
18	324	0.21	0.26	0.12	0.09	0.14	0.64	
19	648	0.10	0.18	0.06	0.04	0.12	0.34	

20

21

1 Table 1b (corresponding to Figure 6)

2

3 N λ_{Smin} λ_{Smax} λ_{min} δ_{Smin} δ_{Smax} R

4

5 *Figure 6a* ($T=450, a=0.8, h=0.4, c=1.7, k=0.35$)

6 162 0.34 0.48 0.30 0.03 0.17 0.19

7 648 0.21 0.32 0.11 0.10 0.21 0.47

8

9 *Figure 6b* ($T=610, a=0.8, h=0.4, c=1.7, k=0.35$)

10 162 0.37 0.47 0.31 0.06 0.16 0.39

11 648 0.24 0.35 0.10 0.14 0.25 0.56

12

13 *Figure 6c* ($T=700, a=0.8, h=0.4, c=1.7, k=0.35$)

14 162 0.35 0.46 0.30 0.05 0.15 0.31

15 648 0.24 0.31 0.10 0.14 0.21 0.70

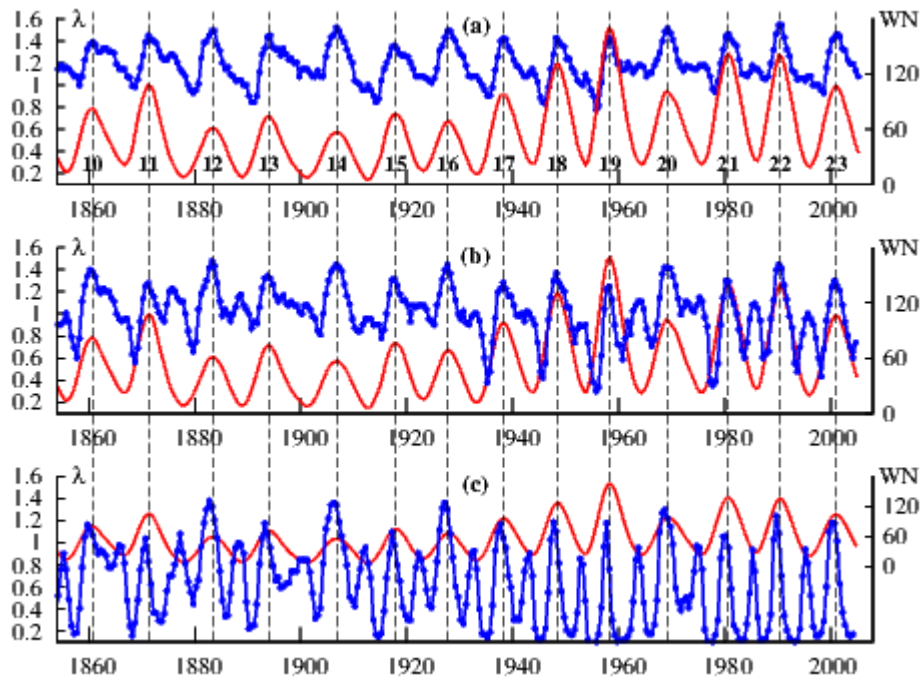
16

17 *Figure 6d* ($T=800, a=0.8, h=0.4, c=1.7, k=0.35$)

18 162 0.36 0.51 0.32 0.05 0.19 0.25

19 648 0.18 0.34 0.10 0.08 0.23 0.35

20

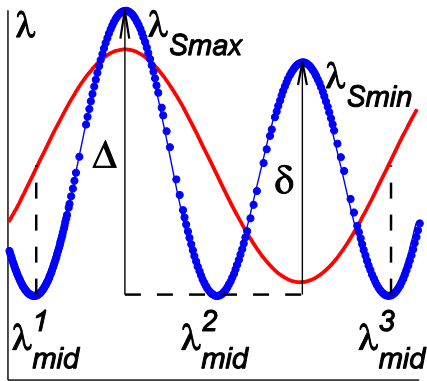


1

2

3 Figure 1. The irregularity index λ (blue) computed in a 4-year sliding window for the
 4 International Sunspot Number (*ISSN*) averaged over 162 (top), 324 (middle), and 648
 5 (bottom) days; embedding dimension $m = 1$. The Wolf numbers averaged first over $N = 162$,
 6 324, and 648 days, and then over 4 years are shown in red, together with solar cycle number.
 7 Dashed black vertical lines are located at the maxima of *ISSN*.

8



1

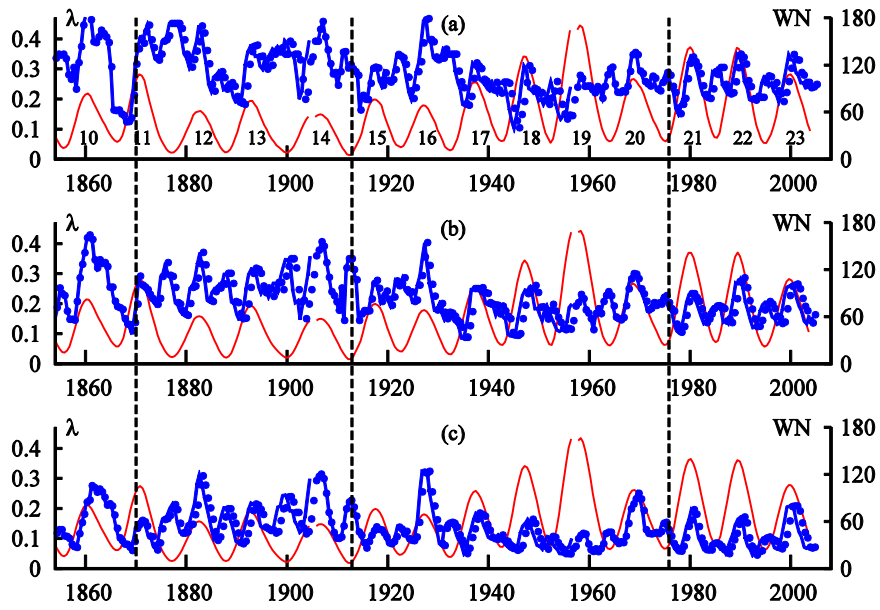
2

3 Figure 2. Construction of $R = \delta_{Smin} / \Delta_{Smax}$ (see text); smoothed artificial signal (red) and its

4 irregularity index (blue); main maxima λ_{Smax} secondary maxima λ_{Smin} , and local minima λ_{mid}^i .

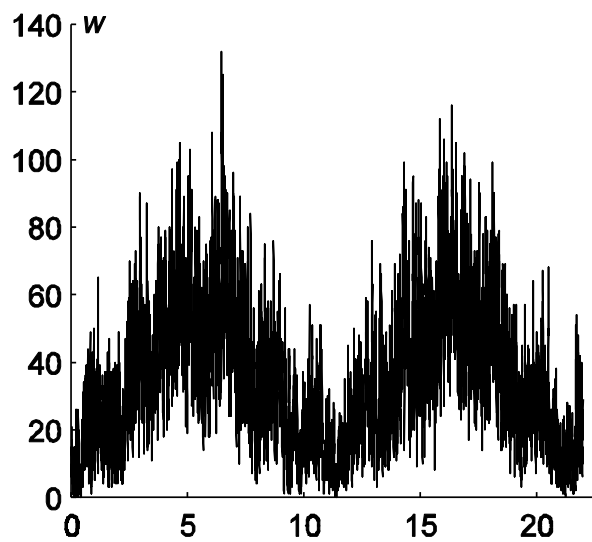
5 Black lines show construction of Δ_{Smax} and δ_{Smin} .

6



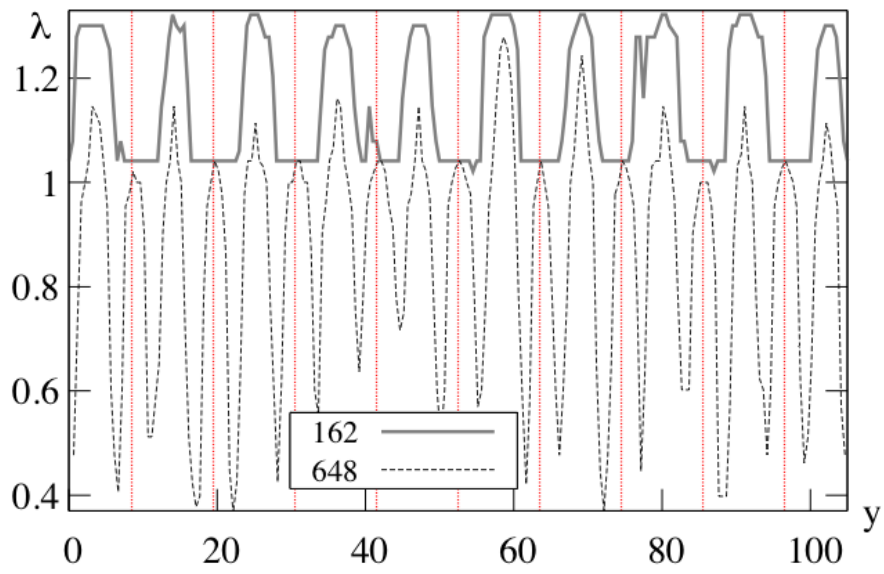
1
2
3
4
5
6
7

Figure 3. Blue curves : the irregularity index λ computed in 4-year sliding window for the Wolf numbers averaged over N days; red curves : the Wolf numbers averaged over N days and then over 1461 days (4 years), where N is 162 (top), 324 (center), and 648 (bottom) days; $m = 2$. Dashed black vertical lines are located at times of possible regime change of λ .



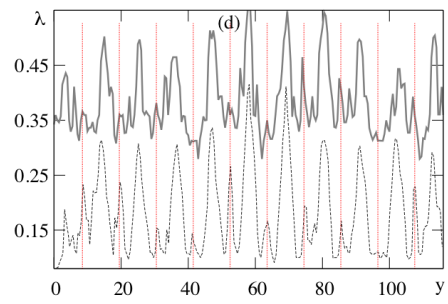
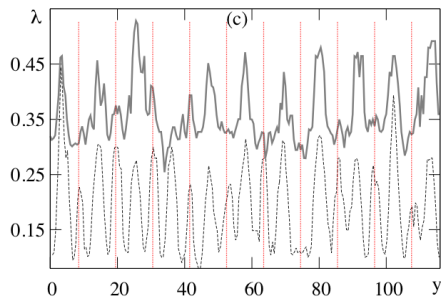
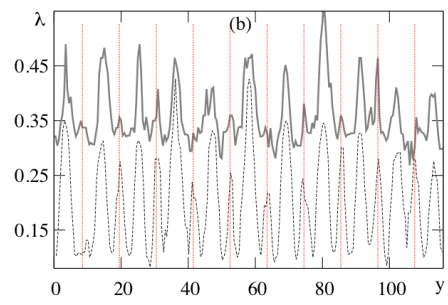
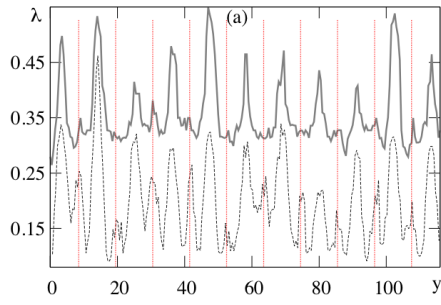
1
2
3
4
5
6

Figure 4. A realization of the AR(1) process introduced in section 3.1, shown prior to smoothing by N days and over the 4 year interval over which it will next be averaged (see text). Model parameters: $a = 0.8$, $h = 0.4$, $k = 0.35$, $c = 1.7$, $T_1 = 11$ yr, $T_2 = 700$ days.



1
2
3
4
5
6

Figure 5: The irregularity index computed in 4-year sliding window for synthetic data averaged over 162 (solid gray) and 648 (dashed black) days ($m = 1$). Model parameters: $a = 0.8$, $h = 0.4$, $k = 0.0$, $c = 1.7$. Red dashed vertical lines at solar sunspot minima.



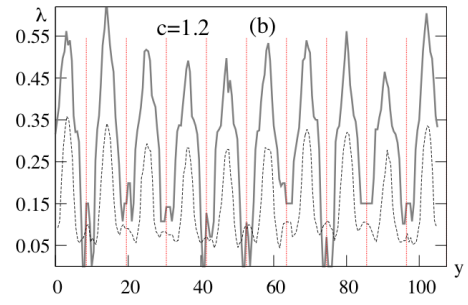
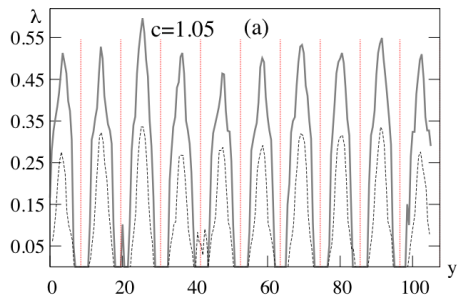
1

2

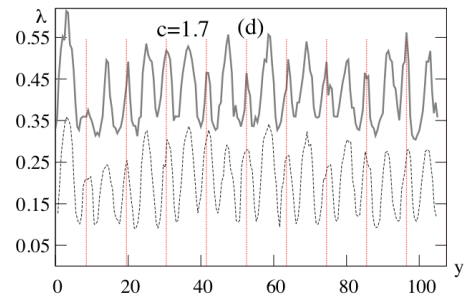
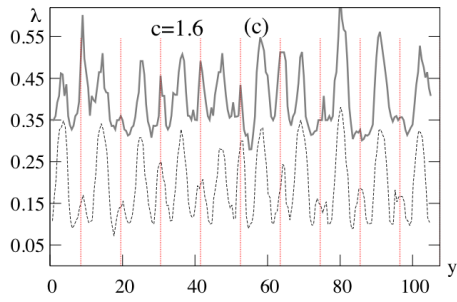
3

4 Figure 6: The irregularity index computed in 4-year sliding window for synthetic data
 5 averaged over 162 (solid gray) and 648 (dashed black) days ($m = 2$). Model parameters: $a =$
 6 0.8 , $h = 0.4$, $c = 1.7$, $k = 0.35$, and intermediate period variation T_2 set at 450 (a), 610 (b), 700
 7 (c), 800 (d) days. Red dashed vertical lines at solar sunspot minima.

8



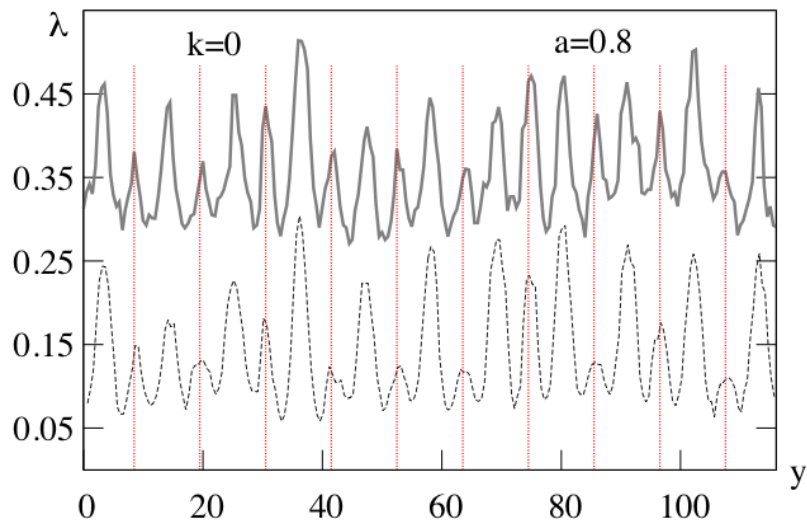
1



2

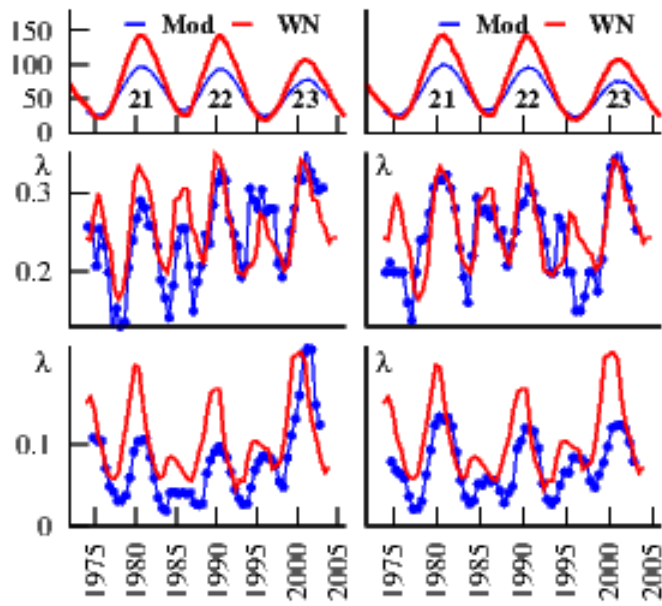
3 Figure 7: The irregularity index computed in 4-year sliding window for synthetic data
 4 averaged over 162 (solid gray) and 648 (dashed black) days ($m = 2$). Model parameters are: a
 5 $= 0.8$, $h = 0.4$, $k = 0$, and $c = 1.05$ (a), 1.2 (b), 1.6 (c) and 1.7 (d). Red dashed vertical lines at
 6 solar sunspot minima.

7



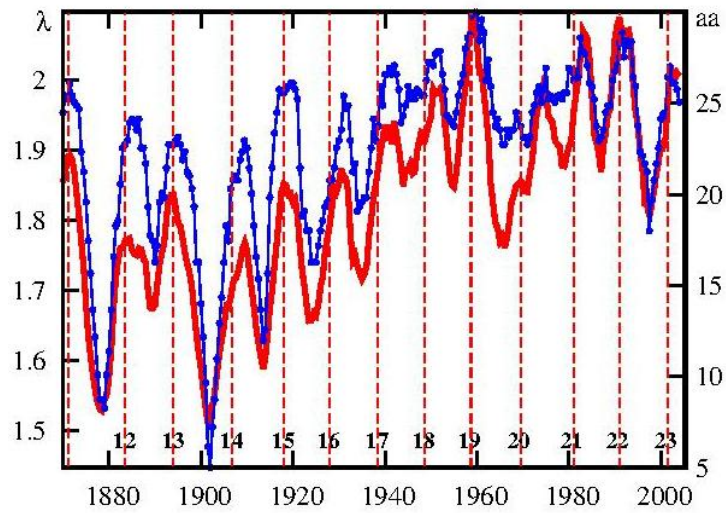
1
2
3
4
5
6

Figure 8: The irregularity index computed in 4-year sliding windows for synthetic data averaged over 162 (solid gray) and 648 (dashed black) days ($m = 2$). Model parameters: $a = 0.8$, $h = 0.8$, $k = 0$, $c = 1.7$. Red dashed vertical lines at solar sunspot minima.



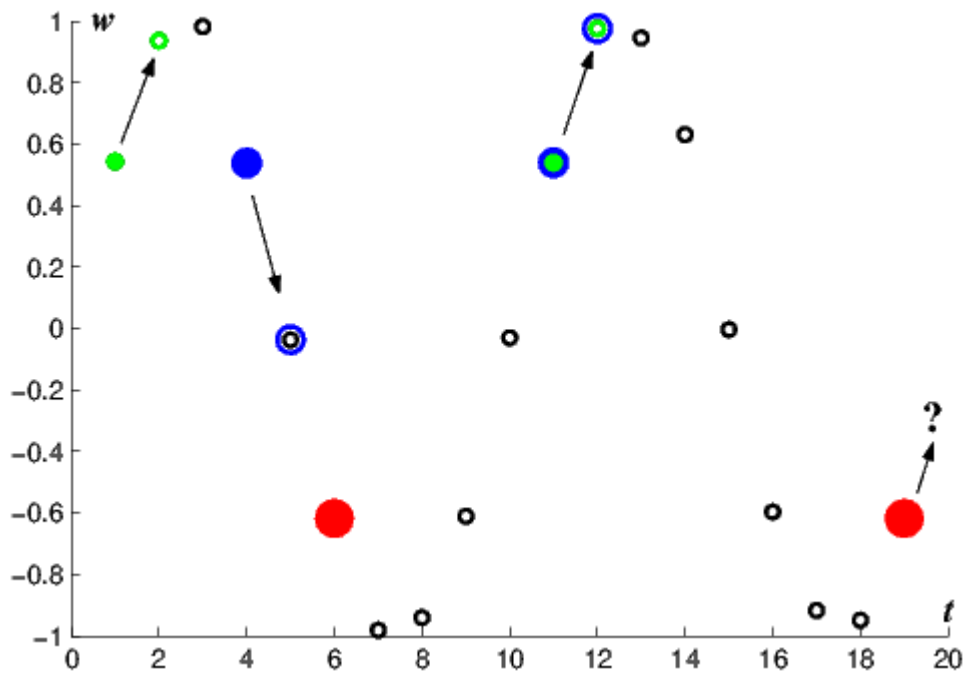
1
2
3
4
5
6
7

Figure 9: Top row: two synthetic signals (blue; see text) and *ISSN* (red) averaged over 4 years. The two columns of the figure are relative to different synthetic signals. The irregularity index ($m = 2$) for model (blue) and *ISSN* (red) series are shown averaged over 162 days (middle row) and 648 days (bottom row). $a = 0.9$, $h = 0.4$, $k = 0$.



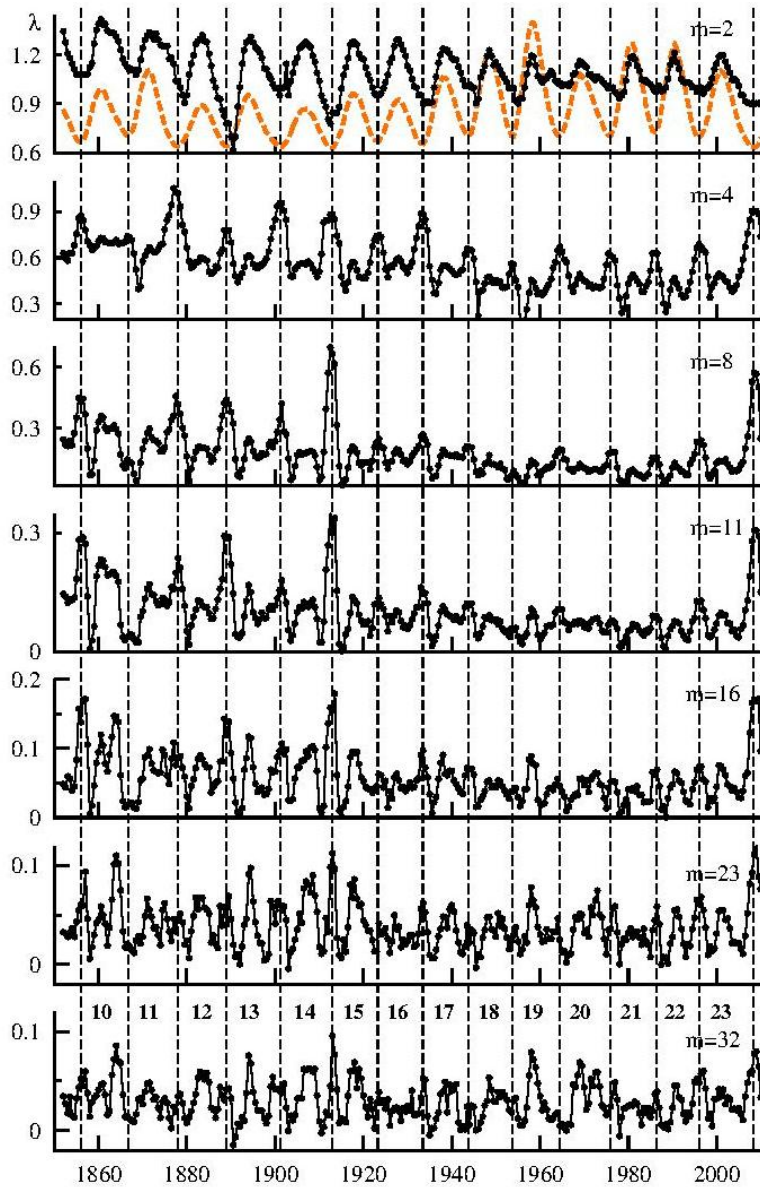
1
2
3
4
5
6

Figure 10. Red curve: the daily *aa* averaged over 4 years. Blue curve: the irregularity index λ computed in a 4-year sliding window with $m = 1$. Vertical dashed lines are at the maxima of Wolf numbers (averaged over 4 years). The number of each Schwabe cycle is indicated.



1
2
3
4

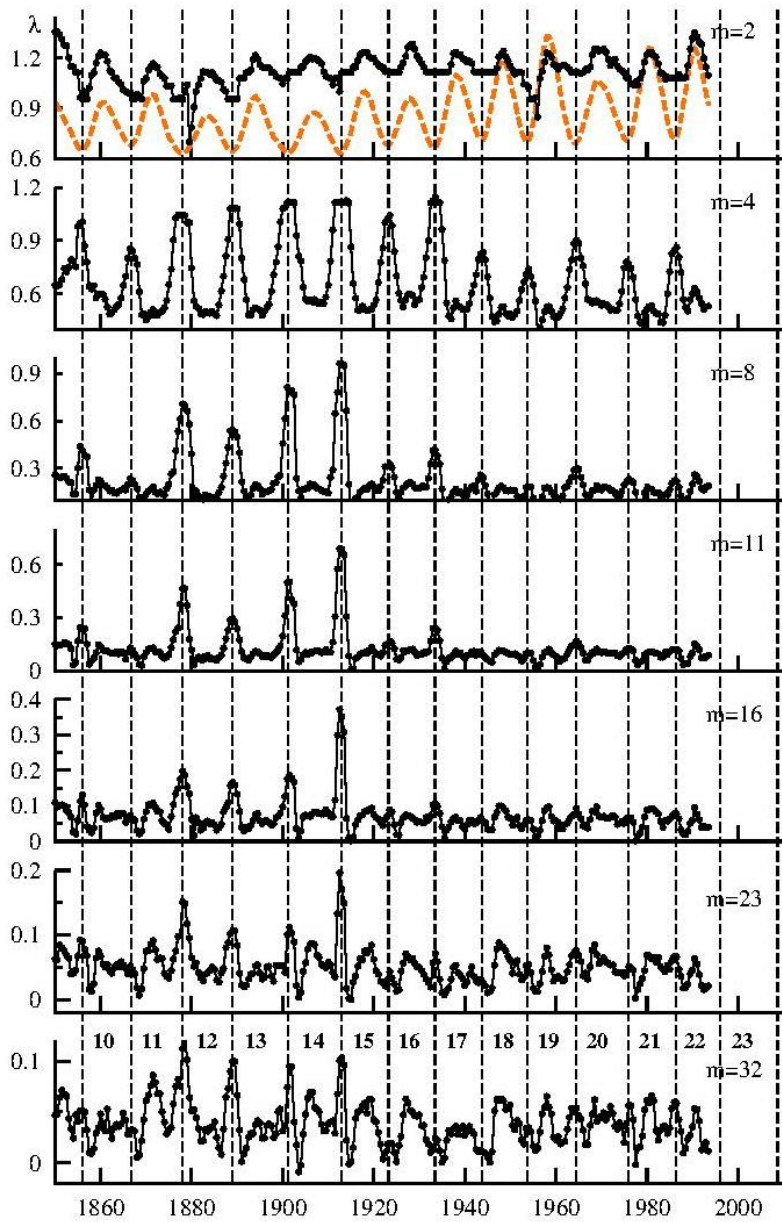
Figure 11: Computation of λ . Synthetic signal vs. time (see text).



1

2 Figure 12. The irregularity index λ computed for *ISSN* within 4-year sliding windows;
 3 the embedding dimension m is indicated; vertical lines are at solar cycle minima.

4



1

2 **Figure 13. The irregularity index λ computed for GSN (Hoyt & Schatten, 1998) within 4-year**
 3 **sliding windows; the embedding dimension m is indicated; vertical lines are at solar cycle**
 4 **minima.**